AIAA'83

AIAA-83-1548

Flowfield Description for the Reaction Control System of the Space Shuttle Orbiter

J.W. Alred, NASA Johnson Space Center, Houston, TX

AIAA 18th Thermophysics Conference

June 1-3, 1983
Montreal, Canada

FLOW FIELD DESCRIPTION FOR THE REACTION CONTROL SYSTEM OF THE SPACE SHUTTLE ORBITER

John W. Alred*
NASA Lyndon B. Johnson Space Center
Houston, Texas

Abstract

The flow field for the Reaction Control System (RCS) jets of the Space Shuttle Orbiter has been calculated from the nozzle throat to the far-field flow region. The calculations involved the use of recently improved rocket engine nozle/plume codes and the source flow analytic model. The flow solution is discussed and used to produce impingement forces and moments for surfaces immersed in the flow. The impingement results are compared to calculations involving previous flow solutions in order to evaluate the impingement effects due to the RCS jets during orbital operations.

Nomenclature

Symbol	Description
A	source flow density proportionality constant
C_p	impingement pressure coefficient
f	source flow angular dependence function
Kn	Knudsen number
P	pressure
$\bar{q}$	dynamic pressure
R	universal gas constant
R_E	nozzle exit radius
r	radial distance from nozzle exit plane
T	temperature
V	velocity

Greek

α	impingement angle
γ	isentropic exponent
ΔF	incremental impingement force
ΔS	incremental surface area
ρ	density
θ	angle from nozzle centerline

Subscripts

CL	indicates centerline value
ρ	indicates density-associated value
V	indicates velocity-associated value

Introduction

Two of the major goals of the Space Transportation System (STS) are the deployment and retrieval of orbital payloads. The ability of the Space Shuttle Orbiter to perform the first task was successfully demonstrated in the STS-5 mission (November 11-16, 1982) during which two satellites were routinely deployed and boosted to their operational orbits. While in orbit, the Space Shuttle Orbiter uses its Reaction Control System (RCS) jets to maneuver. The aft RCS jets also provide the primary vehicle control from deorbit until the control surfaces become effective. However, plume interactions due to the RCS flow field affect both payload operations and Orbiter operations and must be analyzed to successfully perform STS mission objectives.

The use of the forward and aft RCS jets during orbital flight maneuvering produce plume impingement on Orbiter surfaces. The down-firing RCS jets impinge on the nozzles of the Space Shuttle Main Engines (SSME), on the body flap, and on parts of the Orbiter wing. The up-firing jets impinge on the vertical tail while the side-firing RCS impinge primarily on the Orbiter wing. The effect of the plume impingement produces forces and moments that counteract the forces and moments due to the thrust vector of the jet. The RCS jets hence lose effectiveness due to the plume impingement. The impingement losses must be calculated and included in any mission profile.

Plume impingement and contamination are also problems in payload operations, such as payload deployment from the Orbiter, rendezvous maneuvers with an orbiting payload, and payload retrieval. When the Orbiter is engaged in payload operations, extreme caution must be used to minimize RCS plume impingement to the payload. Indeed, studies [1] have shown that plume impingement from the RCS jets can effect the motion of an orbiting payload to the extent that the payload is difficult if not impossible to recover. Again, for successful STS missions, a precise knowledge of the RCS jet flow field is imperative.

The design and operational conditions of an RCS nozzle made computational solutions difficult. With the use of the updated RAMP computer model [2, 3], the RCS nozzle flow solution was obtained. The first section of this paper will discuss the calculation of the RCS flowfield and compare it to previous versions. Once the flow field is described the impingement analysis is performed to obtain the forces and moments needed to answer on-orbit plume

*Member AIAA

interaction questions. The second section of this paper will describe the impingement results as well as the impingement results of previous models. The second part of this paper will also delineate the current and future uses for the latest RCS flow field including tests scheduled in order to acquire on-orbit impingement data.

RCS Flow Field Calculation

The RCS jets are bipropellant rocket motors using monomethylhydrazine (CH_6N_2 or MMH) as a fuel and nitric oxide (N_2O_4) as an oxidizer. The desired flow field of an RCS motor is calculated in four stages:

1. Combustion chamber
2. Nozzle interior flow
3. Near-nozzle-exit plume
4. Far-field flow region

The first calculation involves obtaining the chemical and thermodynamic conditions in the combustion chamber and plume expansion. The thermochemical and transport data for the RCS exhaust flow are obtained using a RAMP-compatible, modified version of the TRANS72 computer model [4,5]. The calculations are made using a chamber pressure of 153 psi and oxidizer-to-fuel (O/F) ratios of 0.8 to 2.2. The combustion chamber and nozzle interior flows are assumed to be in chemical equilibrium with the chemistry frozen at 45.67 psi, corresponding to the Mach 2 contour in Fig. 1 and beyond. The reacting gas solution is passed to the RAMP program to calculate the nozzle flow solution.

The calculation of the nozzle flow field for the RCS jet involves computational techniques heretofore unavailable in RAMP [3]. The geometry of the RCS jet near the nozzle throat has a radius of curvature that caused numerical problems in the transonic flow region, and the O/F ratio in this transonic region is variable. The improved version of RAMP was used to overcome these problems and obtain the nozzle flow solution (Fig. 1 and Fig. 2). The RAMP program automatically invokes the BLIMPJ computer model [6] to calculate the real gas, turbulent, nozzle boundary layer. The boundary layer calculation begins with laminar flow and switches to turbulent flow when the Reynolds number based on momenteum thickness exceeds 250 and uses an input nozzle wall temperature distribution. The boundary layer thickness for the RCS nozzle as calculated by BLIMPJ is .0698 inches. The results of BLIMPJ are stored and subsequently used by RAMP when the latter program is re-executed to produce an exit plane start line that has the results of the inviscid nozzle and boundary layer solutions merged.

Conditions of the nozzle flow solution at the exit plane of the nozzle are input via the start line generated by the RAMP-BLIMPJ-RAMP combination into the MOC computer code [7] to obtain the third flow regime. The MOC program was used as it currently performs a boundary layer expansion more efficiently than the RAMP code [3]. The MOC flow field was generated to 85 exit radii, where the exit radius of the RCS nozzle is 4.8 inches. This limit was determined by the Bird "continuum breakdown parameter." [8] The flow can now be converted to a free molecular plume expansion.

To extend the knowledge of the flow field from the continuum region (near-nozzle-exit) to the free molecular region, the source flow plume model [9] is used. The source flow model assumes the gases diverge radially as from a point source. From this assumption and the conservation of momentum, the density of the flow field varies as an inverse square of the radial distance from the exit nozzle, i.e.,

$$\text{with } \rho = \frac{A(R_E)^2 f(\theta)}{r^2} \tag{1}$$

and

$$f(\theta=0) = 1. \tag{2}$$

In terms of a ratio,

$$\frac{\rho_1}{\rho_2} = \frac{f(\theta_1)}{f(\theta_2)} \cdot \frac{(r_2)^2}{(r_1)^2}. \tag{3}$$

By using calculated densities given by MOC, a graphical representation for $f(\theta)$ can be obtained (Fig. 3). Also from the MOC results and the expression for density ratios, values for densities along the nozzle centerline may be obtained (Fig. 4). Similar graphical representations can be performed for the gas velocity as shown in Figs. 5 and 6.

To use the source flow results, one must specify the radius from the center of the exit plane and the angle from the centerline to the point where values are to be derived. The density at the specified radius and along the centerline can be obtained from the graph in Fig. 4. This density represents the centerline density denoted ρ_{CL}. The density at the desired angle can be obtained by multiplying ρ_{CL} by $f_\rho(\theta)$. Symbolically, this process is represented as

$$\rho(r,\theta) = \rho_{CL}(r) f_\rho(\theta) \tag{4}$$

and, similarly,

$$V(r,\theta) = V_{CL}(r) f_V(\theta). \tag{5}$$

Having the values for $\rho(r,\theta)$ and $V(r,\theta)$, one can now calculate other desired flow field parameters from thermodynamic relations. For example, other calculable parameters are

Temperature $$\left(\frac{T_1}{T_2}\right) = \left(\frac{\rho_1}{\rho_2}\right)^{-1/\gamma} \quad (6)$$

Pressure $$P = \rho RT; \quad (7)$$

Dynamic Pressure $$q = 1/2\ \rho V^2; \quad (8)$$

and

Newtonian Impact Incremental Impingement Force

$$F = C_p q \Delta S \sin^2\alpha. \quad (9)$$

where C_p is the pressure coefficient which typically varies from 2 to 4, depending on accommodation assumptions at the impact surface.

An interpolative computer program has been written to automatically perform the look-up analysis described above. A comparison of dynamic pressure from this analysis with MOC-generated results for two previous RCS plume flow solutions is shown in Fig. 7. The previous solutions have been labeled constant O/F and variable O/F. The constant O/F model refers to the first complete RCS flow field used to consider the on-orbit plume interaction questions. The plume was generated by the MOC program with an exit plane start line with O/F = 2.2 and no boundary layer. This exit plane start line was constructed by a one-dimensional analysis from the RCS throat. The variable O/F plume was generated by upgrading the constant O/F exit plane start line to include O/F ratios from 0.8 to 2.2 and to include boundary layer effects as indicated by test data. However, due to the rapid progress in the development of RAMP, the variable O/F results were not used to consider plume impingement. As seen in Fig. 7, the RAMP-generated data agrees well with the variable O/F results initially and then parallels the constant O/F values.

On-Orbit RCS Plume Interactions

Two applications of the RCS flow solution are the RCS plume impingement on the Orbiter during orbital flight maneuvering and RCS plume impingement to free flying payloads in the vicinity of the Orbiter during proximity operations. To assess the impacts of the new RCS plume model on these applications, the RAMP calculated flow solution as well as the previous flow solutions was used in three impingement calculations. The first two cases involved using the PLIMP [10] plume impingement model to compare the models with a simple geometry. The last case calculates and compares impingement moments and forces on Orbiter surfaces due to the aft RCS jets.

A surface immersed in the exhaust plume of a rocket motor experiences impingement from gases that may vary from extremely dense to extremely rarefied. The impingement loads calculations must be applicable in the continuum, translational, and free molecular flow regimes. These regimes are described by the ratio of the number of intermolecular collisions to the number of surface collisions, that is, the ratio is low in the transitional regime, very high in the continuum regime, and nearly zero in the free molecular (molecular collisionless) region. These flow regimes are most commonly differentiated by the Knudsen number, Kn, which is a dimensionless parameter that is the ratio of the mean free path relative to a reference length. The flow regimes are usually defined by the following values:

$0.0 \leq Kn \leq 0.01$	Continuum
$0.01 \leq Kn \leq 10.0$	Transitional
$10.0 \leq Kn \leq \infty$	Free Molecular

For the comparison cases of this paper, the continuum regime was utilized in impingement calculations. As referenced in equation (9), the continuum flow impingement was calculated using the modified Newtonian impact theory.

The first comparison was made by calculating the forces on a square flat plate whose center was placed on the nozzle centerline (Fig. 8). The impingement forces were obtained from PLIMP and reflect the radial structure of the plume flow. The distance along the nozzle centerline from the nozzle exit plane to the face of the plate was varied from 50 inches to 500 inches by increments of 50 inches. The comparison of impingement forces between the RAMP and constant O/F is shown in Fig. 9 while the RAMP and variable O/F comparison shown in Fig. 10. The values initially differ due to the artificial construction of the previous models but converge as expected, in the source flow region. The latter fact is more clearly illustrated by a comparison of a source flow model based on the constant O/F plume flow solution and the source flow model as updated with the RAMP flow solutions (Fig. 11).

The second comparison was made by again calculating the forces on a square flat plate whose center is now offset from the nozzle centerline but with the unit normal of the plate parallel to the centerline (Fig. 12). In this case, the impingement forces and moments from PLIMP reflect the angular or theta structure of the flow solutions. All moments are referenced to the center of the plate. The distance from the center of the plate to the nozzle centerline is varied from 0 inches to 500 inches in increments of 50 inches. The constant O/F flowfield overpredicted the density profile in an attempt to add boundary layer effects. This effect can be seen in the impingement forces comparison in Fig. 13 and the moments comparison in Fig. 14. The RAMP-generated flow solution and the previously generated variable O/F plume model included effects due to the boundary layer as can be seen in the forces and moments comparisons (Fig. 15 and Fig. 16, respectively). The previous source flow model based on the constant O/F flow solution, however, underpredicts the mass flow from the boundary layer that is evident in the RAMP-updated source flow model. This fact is noted in the comparisons of Figs. 17 and 18.

To predict the magnitude of RCS plume impingement on the Orbiter during orbital flight maneuvering, the PLIMP model was used in

conjection with the aft surface geometry of the Orbiter. The forces and moments due to impingement were calculated for a down-firing, and up-firing, and a side-firing jet. The calculations for each jet were made with each of the three flow solutions discussed in this paper. The moments due to plume impingement are referenced to the Orbiter's center of gravity. The impingement loads are tabulated in Table 1 as a function of RCS jet type and plume model. As expected from the previous comparisons, the values derived from the constant O/F flow solution are higher than the other two flow solutions, which agree with each other quite well. From the values of Table 1, the RAMP-derived impingement loads predict that the aft RCS jets are more effective (less impingement) than orginally thought. This fact agrees with flight data from RMS strain gauges on STS-4.

Further actual on-orbit measurements are currently planned at the NASA Johnson Space Center (JSC) for Orbiter flights STS-6 and STS-7. The Aerodynamic Coefficient Identification Package (ACIP) aboard the Orbiter Challenger will provide high resolution accelerometer and rate data of Orbiter motion during single RCS jet firings. From this data, the magnitude of RCS aft impingement loads will be determined and compared to the predicted values of Table 1.

The SPAS-01 RCS plume impingement is scheduled for STS-7. This experiment involves measuring the plume impingement on a free-flying satellite, here the first Shuttle Pallet Satellite (SPAS-01), due to firings of a single RCS motor. The SPAS-01 has high resolution accelerometers and rate gyros that will measure the perturbation on the satellite due to the plume environment. This data will be used to verify the impingement values predicted by the current satellite plume impingement model.

Conclusions

The latest improvements to existing computer models (RAMP) have been utilized in the calculation of the flow field for the RCS jets from the nozzle interior to the far-field flow regime. The flow solutin is needed to answer a wide range of questions arising during Space Shuttle Orbiter operations.

Comparisons between the newly calculated RCS flow field and previous models show expected results based on the construction of the previous models. The RAMP-generated RCS flow field predits less Orbiter impingement and more effective aft RCS jets during on-orbit flight maneuvering. This prediction agrees with low resolution flight data from STS-4. More data of higher resolution is needed to examine the veracity of the current RCS model.

A test program is currently planned at JSC to obtain impingement data for Orbiter on-orbit maneuvering and Orbiter/payload proximity operations. The data from these tests will be used to verify existing plume models.

References

1. Kanipe, D., "Analysis of Plume Impingement Effects During Orbiter Satellite Rendezvous," JSC Memorandum EX32/7509-175, Johnson Space Center, Houston, Texas, September 11, 1975.

2. Penny, M. M., et al., "Supersonic Flow of Chemically Reacting Gas-Paraticle Mixtures - Volume II - RAMP, a Computer Code for Analysis of Chemically Reacting Gas-Particle Flows," LMSC-HREC TR D496555, Lockheed Missiles and Space Co., Huntsville, Alabama, January 1976.

3. Smith, S. D., "Improvements of Rocket Engine Plume Analysis Techniques - Final Report," LMSC HREC TR D784753, Lockheed Missiles and Space Co., Huntsville, Alabama, January 1982.

4. Svehla, Roper A., and McBride, B. J., "FORTRAN IV Computer Program for Calculation of Thermodynamic and Transport Properties of Complex Chemical Systems," NASA TN D-7056, Lewis Research Center, Cleveland, Ohio, 1973.

5. Gordon, Sanford, and McBride, Bonnie J., "Computer Program for Calculation of Complex Chemical Equilibrium Compositions, Rocket Performance, Incident and Reflected Shocks, and Chapman-Jouget Detonations," NASA SP-273, Lewis Research Center, Cleveland, Ohio, 1968.

6. Evans, R. M., "BLIMP-J User's Manual," UM-75-64, Aerotherm, Mountain View, California, July 1975.

7. Smith, S. D., and Ratliff, A. W., "User's Manual - Variable O/F Ratio Method of Characteristics Program for Nozzle and Plume Analysis," LMSC-HREC D162220-IV, Lockheed Missiles and Space Co., Huntsville, Alabama, June 1971.

8. Bird, G. A., "Breakdown of Continuum Flow in Freejets and Rocket Plumes," in Rarefied Gas Dynamics: Proceedings of the 12th International Symposium, July 1980, pp. 681-694.

9. Simons, Girard A., "Effect of Nozzle Boundary Layers on Rocket Exhaust Plumes," AIAA J., Vol. 10, No. 11, pp. 1534-1535, November 1972.

10. Ratliff, Alan W., "Rocket Exhaust Plume Computer Program Improvement - Volume I - Final Report," LMSC-HREC D162220-I, Lockheed Missiles and Space Co., Huntsville, Alabama, January 1972.

Table I Comparison of Orbiter impingement values.

JET	MODEL	F_X	F_Y	F_Z	M_X	M_Y	M_Z
Down Firing Jet	RAMP	-25.5	-165.6	-13.3	1769.	274.3	-6284.
	Variable O/F	-24.1	-160.7	-11.5	1748.	213.9	-6071.
	Constant O/F	-36.1	-232.7	-26.3	2562.	675.0	-8718.
Up Firing Jet	RAMP	0.31	-1.13	-39.3	-982.0	1537.	-57.4
	Variable O/F	0.31	-1.38	-47.9	-1207.	1856.	-68.1
	Constant O/F	-0.09	-2.20	-76.2	-1857.	2929.	-94.1
Side Firing Jet	RAMP	-1.31	-10.68	0.65	319.2	-57.3	-295.3
	Variable O/F	-1.61	-13.05	0.77	389.9	-69.5	-36.7
	Constant O/F	-2.83	-23.01	1.41	675.0	-1226.	-64.6

- Forces in units of lbs.
- Moments in units of ft-lbs.
- Moments referenced to Orbiter c.g.

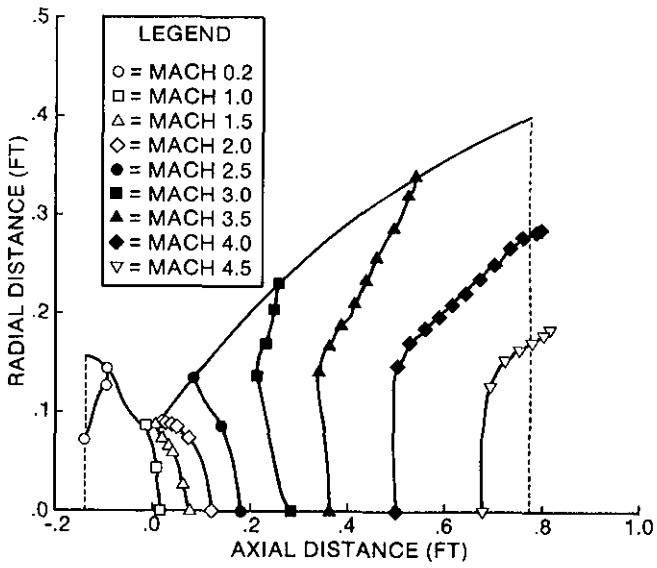

Fig. 1 RCS nozzle interior flow field Mach contour.

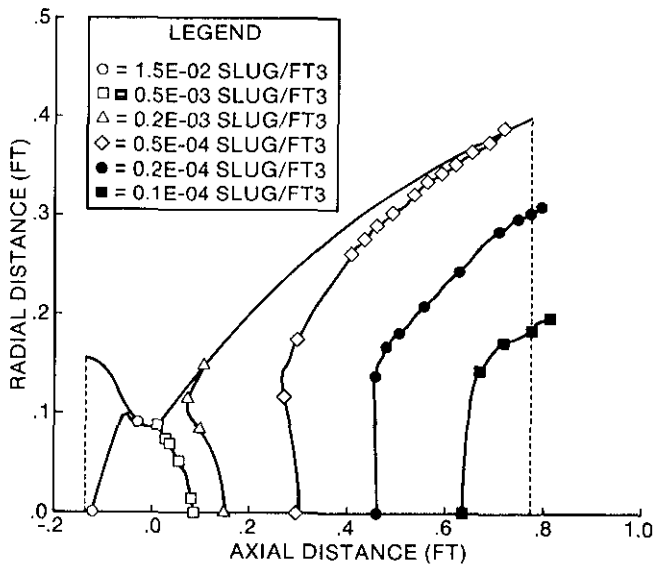

Fig. 2 RCS nozzle interior flow field density contours.

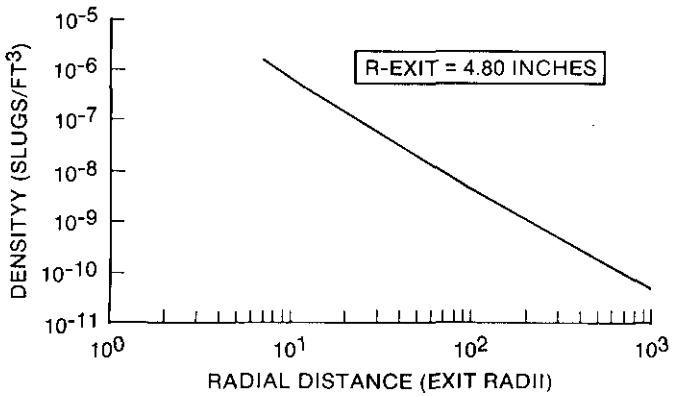

Fig. 3 RAMP-to-source flow RCS plume radial profile for density.

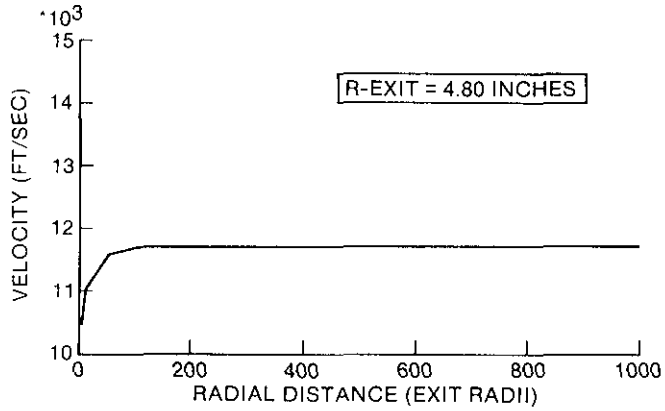

Fig. 4 RAMP-to-source flow RCS plume radial profile for velocity.

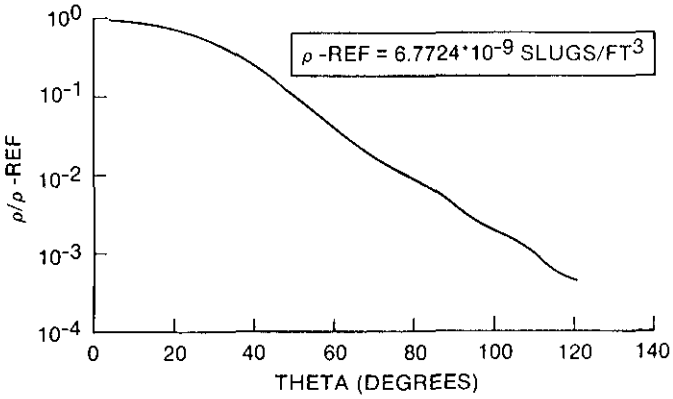

Fig. 5 RAMP-to-source flow RCS plume theta profile for density.

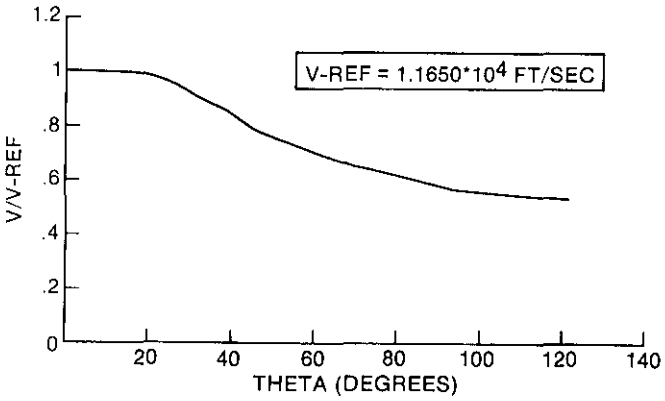

Fig. 6 RAMP-to-source flow RCS plume theta profile for velocity.

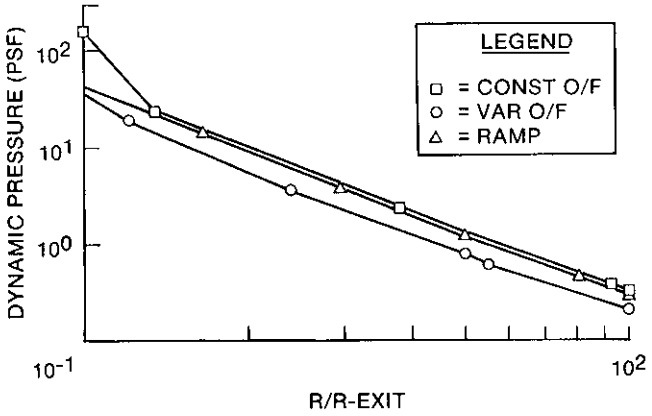

Fig. 7 Comparison of RCS plume models using dynamic pressure.

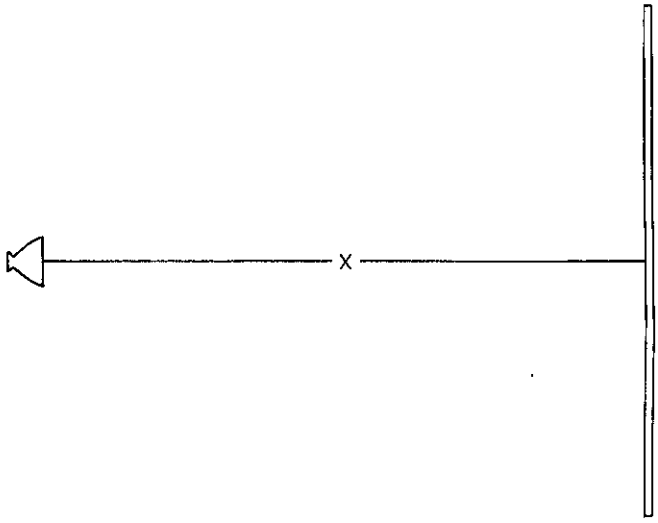

Fig. 8 Radial test case geometry plume impingement on 100 in. by 100 in. flat plate.

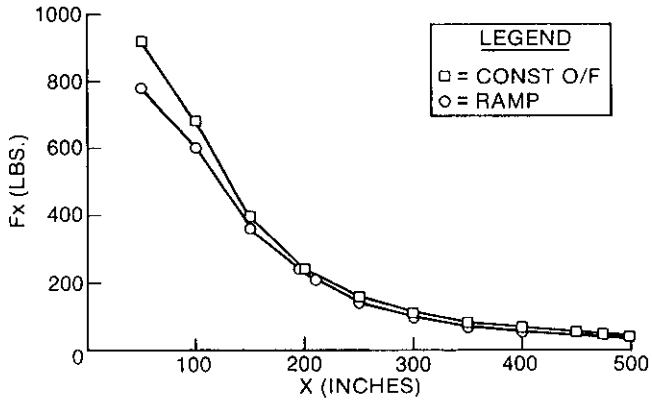

Fig. 9 Radial comparison of RAMP and constant O/F flow fields using impingement forces.

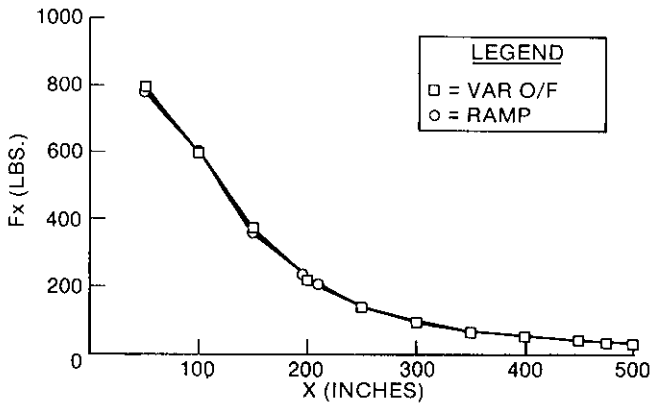

Fig. 10 Radial comparison of RAMP and variable O/F flow fields using impingement forces.

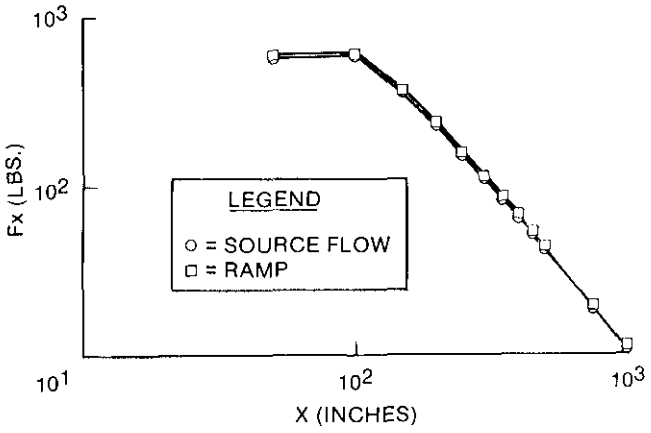

Fig. 11 Radial comparison of source flow model to RAMP-updated model using impingement forces.

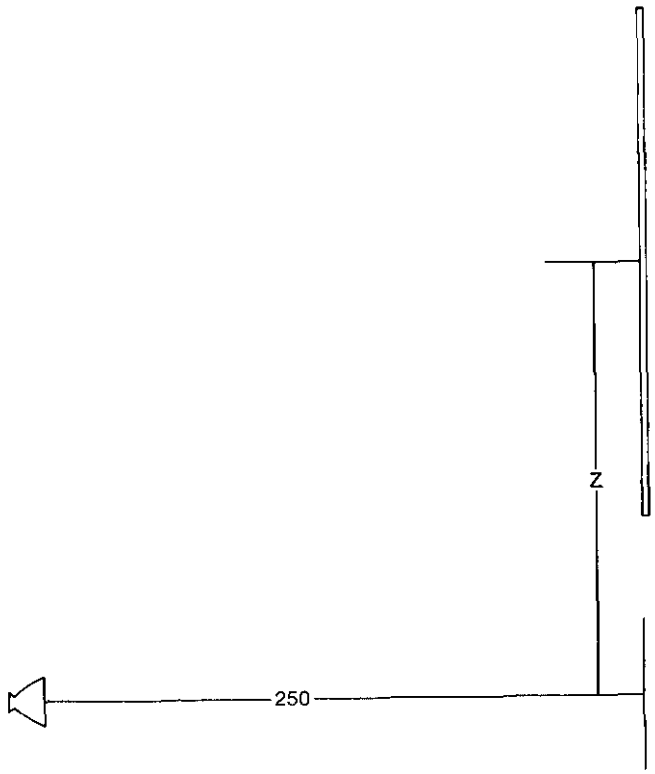

Fig. 12 Angular test case geometry impingement on a 100 in. by 100 in. flat plate.

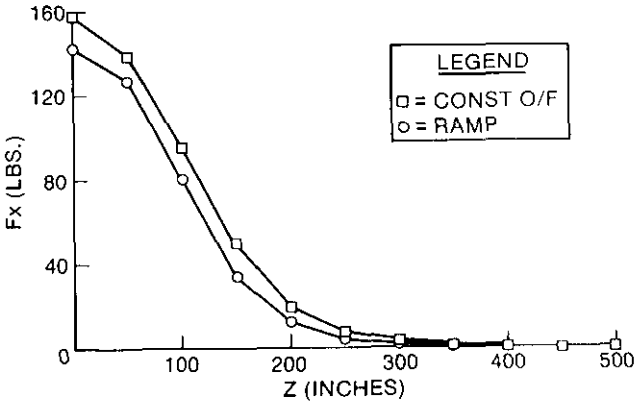

Fig. 13 Angular comparison of RAMP and constant O/F flow fields using impingement forces.

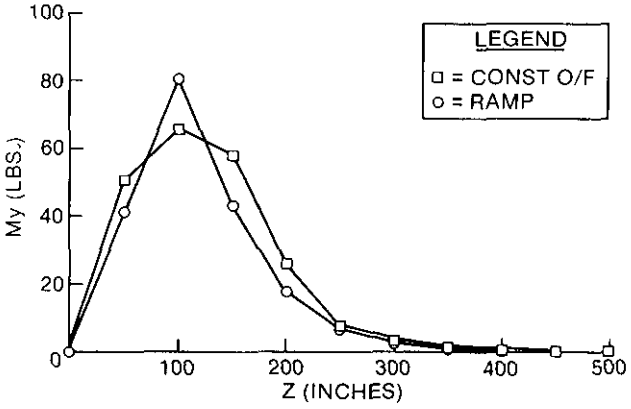

Fig. 14 Angular comparison of RAMP and constant O/F flow fields using impingement moments.

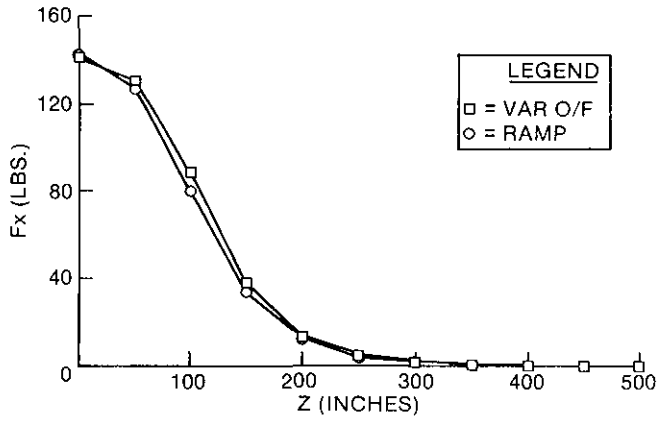

Fig. 15 Angular comparison of RAMP and variable O/F flow fields using impingement forces.

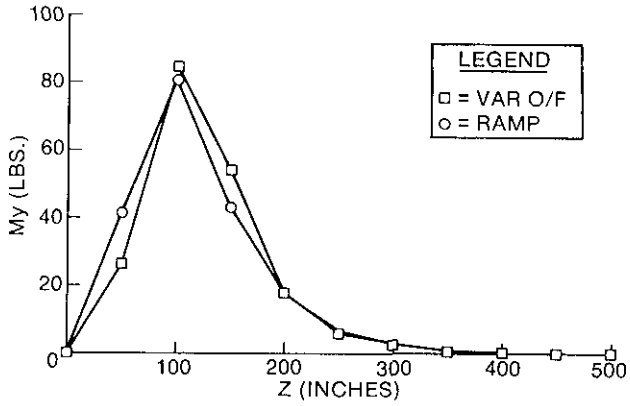

Fig. 16 Angular comparison of RAMP and variable O/F flow fields using impingement moments.

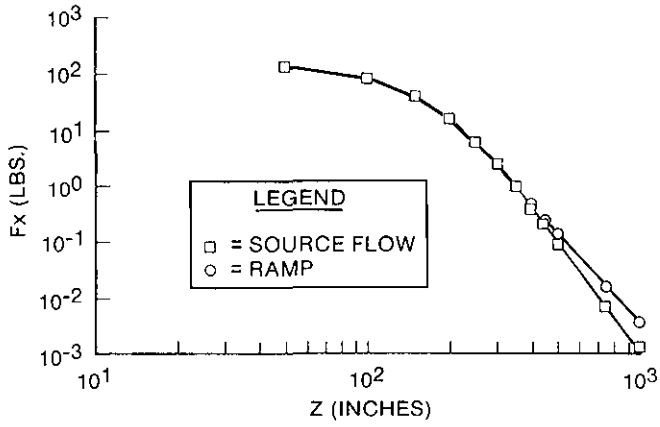

Fig. 17 Angular comparison of source flow model and RAMP-updated model using impingement forces.

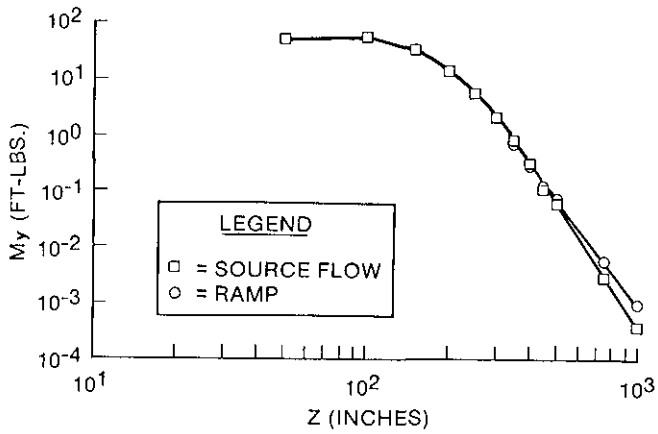

Fig. 18 Angular comparison of source flow model and RAMP-updated model using impingement forces.